To appear in Int. J. Impact Engineering, 2007

Transverse impact of free-free square aluminum beams: an experimental-numerical investigation

A. Dorogoy and D. Rittel (*)

Faculty of Mechanical Engineering, Technion – Israel Institute of Technology

32000 , Haifa, Israel

ABSTRACT

A combined experimental- numerical analysis was performed to model transverse impact of free-free square aluminum beams loaded at different locations along their length. The applied impact load was obtained from tests carried out on a single Hopkinson pressure bar. The 3D elastic-plastic numerical simulations show that the plastic deformation, adjacent to the impact location, is due to combined dominant bending and stretching modes. Most of the plastic deformation is confined to the impact zone but some partial additional plastic hinges are observed to develop. The plastic strain magnitude and distribution near the impact zone is similar for all tested impact locations, but higher for the more symmetrical impacts. The conversion of impact energy into kinetic, elastic strain energy and plastic dissipation work is characterized for various impact locations along the beam. It is observed that symmetrical impact results in higher plastic dissipation and lower kinetic energy as opposed to unsymmetrical impact. Between 50% and 72% of the applied energy is converted into plastic dissipation energy.

Keywords: aluminum beam, large strain, Hopkinson bar, elastic-plastic material, finite elements, transverse impact

---

(*) Corresponding author: *merittel@tx.technion.ac.il*

1. **Introduction**

The dynamic inelastic behavior of beams has been the subject of many investigations, as shown by Jones [1]. Analytical solutions have been developed for *transversely* impacted beams. These solutions usually apply the classical beam theory which assumes small strains, displacements and rotations. The solutions are usually for a specified pressure pulse which can be step-like, rectangular or triangular. Moreover the material is usually assumed to be *rigid perfectly plastic*.

When the beam is supported, most of the applied energy is converted to strain energy, which results in relatively large plastic deformations. By contrast, when the beam is not supported, the external work is transformed into kinetic and elastic strain energy, as well as plastic dissipation.

A free-free beam subjected to central pulse loading was first studied by Lee *et al* [2], with the simplified assumption of a rigid plastic material. The authors stated that the rigid plastic assumption can be expected to provide a satisfactory approximation to the real elastic-plastic problem if the final strains are large with respect to elastic strains. This requires that the plastic work done in the central plastic hinge should be much larger than the maximum stored elastic energy of the bent beam subjected to the limit moment.

Jones and Wierzbicki [3] developed a theoretical procedure to analyze free-free beams subjected to dynamic pressure load. Exact theoretical solutions for a uniform beam under triangular and step pressure pulse were presented. Their solution relies on the classical beam equations and assumes again that the beam is made from a rigid-perfectly plastic material. It also assumes small strains and negligible elastic effects. Jones and

Wierzbicki [3] concluded that it is more difficult to break a free-free beam, as found in space structures, than a supported beam because only ~25% of the external energy is converted into plastic work. The remaining 75% of the energy causes a rigid body acceleration of the beam.

Yang *et al.* [4] studied the small deflection response of a rigid perfectly plastic free-free beam subjected to a concentrated step load at any cross section along its span, and concluded that no less than 2/3 of the input energy is transformed into kinetic energy, meaning that the plastic energy dissipation in the plastic hinges is always less than 1/3 of the total input energy.

Yu, *et al.* [5] presented a dynamic analysis of an *elastic-plastic* free-free beam subjected to impact by a projectile at its mid span, or to triangular distributed impulse along the beam. Their governing equations, which were based on a small deflection formulation, were solved numerically. Their results were compared with the instantaneous experimental recordings using high speed photography, and good agreement was reported. These authors concluded that an elastic-plastic analysis is necessary to provide a more accurate prediction on the plastic dissipation and possible failure of the dynamically loaded free-free beams.

Yang and Xi [6] conducted an experimental-theoretical study of free-free beams subjected to impact at any cross-section along its span. Their theoretical model assumes an elastic plastic material with linear strain hardening. These authors concluded that the energy partitioning is different for symmetrical and unsymmetrical impacts. The free-free beam will dissipate more plastic work for a symmetrical impact, so that the latter results in greater damage and failure.

From the above-mentioned works, it appears that accurate characterization (without any simplifying assumptions, not even Kirchhoff assumptions) of the plastic damage and energy partitioning for low energy transverse impacts still needs to be carried out. Therefore, we present a hybrid experimental-numerical investigation of free-free aluminum square beams subjected to transverse impact at four different locations along their length. The impact energy is low, less than 0.75 the elastic energy storage capacity of the beams, and the elastic strain is not neglected. Hence, a 3D transient numerical elastic-plastic analysis for large strains is performed. The impact load is applied and measured using a single Hopkinson bar apparatus. The measured experimental load is used as an input into the numerical simulations. The amount of damage and the energy partitioning for the four impact locations is investigated.

The first part of the paper describes the experimental setup and results, while the second part describes the numerical procedures and results. These two parts are followed by a summary and concluding remarks.

Nomenclature

x,y,z	cartesian coordinates
b,h,L,d,V	geometrical parameters of the beam : width, height, length, diameter and volume.
E , E_p	elastic modulus, bilinear plastic modulus
ν	Poisson's ratio
ρ	density
σ_Y	yield stress

W_i	applied impact energy
W_k	kinetic energy of the whole beam
W_e	elastic strain energy of the whole beam
W_p	Plastic dissipation energy in the whole beam
$W^e_{\max}$	Maximum elastic energy storage capacity of the beam
R	Ratio between the applie impact energy to the maximum elastic energy storage capacity of the beam

2. Experimental setup and results

2.1 Experimental setup

Four 6061-T651 aluminum alloy beams were transversely impacted using a single Hopkinson pressure bar apparatus (Kolsky, [7]). The aluminum beams had a square cross section of $b \times h = 12.7 \times 12.7 \quad [mm^2]$, and a length of $2L = 0.5\,m$. The beam was impacted at four different locations (figure 1): $\frac{x}{L} = 0.0, 0.40, 0.67$ and 0.90 respectively. The experimental setup consisted of an Hopkinson bar that is brought in contact with the beam at $(x, y, z) = (0, 0, h/2)$ (figure 2). In this one-point impact experiment, a cylindrical striker, fired by the air gun, impacts the Hopkinson bar and generates stress waves that travel along the bar and impinge upon the beam. The (1D) stress waves are recorded by strain gages mounted on the Hopkinson bar. These are used to calculate the applied load on the specimen as well as the striker velocity [7]. The striker diameter and length are: $d^{\phi} \times L_s = 12.7 \times 207 \quad [mm]$ respectively. The incident bar diameter and length are: $d^{\phi} \times L_H = 12.7 \times 717 \quad [mm]$. The striker and the bar are made of Maraging 250 hardened steel. Two strain gages are cemented on the incident bar, 300 mm from the edge that is in contact with the specimen. Recording applied loads is not possible when beams are loaded by various projectiles (e.g. bullets), so that the advantage of impact loading using a single Hopkinson bar apparatus is clear, as the load is both applied and measured with the same apparatus.

2.1 Experimental results

The main experimental results consist of four curves that describe the impact load for the four different impact locations, x/L = 0, 0.4, 0.67 and 0.9, as shown in figure 3. The approximations of these graphs, which were used in the subsequent numerical analyses are indicated by various symbols. For the four experiments, the typical striker velocity was 33 m/s.

3. Numerical analysis

3.1 Numerical procedure

Abaqus explicit version 6.6-1 [8] was used to simulate the impacted beams. 3D transient elastic- plastic analyses with geometrical nonlinear capabilities were applied. The mesh consisted of 71424 elements of type C3D8R. These elements are linear, brick shaped with 8 nodes which use reduced integration and hourglass control [8]. The element size used is ~1.05 mm in size. This element size insures numerical convergence i.e. further decrease of mesh size does not change the results substantially. The mesh near the edge of the beam is seen in figure 4a.

The aluminum beam was assumed to be an elastic plastic material with bilinear isotropic hardening. The following material properties were used: density $\rho = 2700\ Kg/m^3$, Young's modulus $E = 68.9\ GPa$ and Poisson's ratio $\nu = 0.33$. The plastic modulus was taken to be $E_p = 133\ MPa$ and the yield stress $\sigma_y = 276\ MPa$. The time is normalized

by $t^* = \frac{t C_v}{L}$ where $C_v = \sqrt{E/\rho}$ is the longitudinal wave speed in aluminum and $L = 0.25$ m is half the length beam. The normalized time is a measure for the number of times a stress wave can travel along the half length of the beam. The analyses were stopped at $t^* = 101$ (5 ms) while the duration of the impact was approximately $t^* = 1.82$ (90 μs). The load was applied as a uniform distribution of pressure on a rectangle 12.7 mm * 12.7 mm shown in figure 4b. Finally, the beam was not supported, thus allowing for rigid body motion.

3.2 Numerical results

The numerical results consist of two parts. The first part describes the beam deformation, emphasizing plastic strains. First the calculated beam shape is introduced. Next, the distribution, magnitude and evolution of the plastic damage are described and quantified. The second part addresses energy partitioning in the whole beam up to $t^* = 101$.

3.2.1 Plastic deformations

The transverse displacements of the beam (u_z) along its length $-L \le x \le L$ at $(y, z) = (0, h/2)$ are plotted in figure 5, for the following impact locations: x/L = 0, x/L = -0.4, x/L = -0.67 and x/L = -0.9 respectively. The deformed beam shape is plotted for five distinct time values: $t^* = 20.2, 40.4, 60.6, 80.8$ and 101 (1, 2, 3, 4 and 5 ms, respectively). It can be observed that higher values of x/L results in higher displacements. This can be explained by the fact that, when the impact is closer to the edge of the beam,

larger rotations occur, which add to the translation and cause higher overall displacements.

The deformed meshed beam with a cut view at the impact location of $x/L = 0$ at time $t^* = 101$ is seen in figure 6. The equivalent plastic strain distribution is plotted on the outer surfaces showing the hinge shape, and indicating that the extent of the hinge is approximately twice the beam width.

The variation of the equivalent plastic strain at point P $(x/L, y/h, z/h) = (0, 0, -1/2)$ for impact location of $x/L = 0$ is plotted in figure 7. It is observed that most of the plastic deformation develops during the early stages of loading. When loss of contact occurs between the Hopkinson bar and the beam ($t^* > 1.82$), stress waves which travel along the beam continue to alter the plastic deformation. At $t^* = 101$, the plastic deformation of point P can be considered as completed.

The distribution of the total bending strain ε_{xx} on a path which passes trough the point P is plotted in figure 8. The path is shown in figure 6, and it stretches between $-1/2 \le z/h \le 1/2$. The distribution is for time $t^* = 101$, at $x/L = 0, 0.4, 0.67$ and 0.9 respectively. This figure shows that the impact causes bending deformation at all the impact locations. Bending is accompanied by some stretching since the positive strains at $z/h = -0.5$ are slightly larger in absolute value than the strains on the impacted face at $z/h = 0.5$. The distribution is not a straight line, which indicates that the assumption of the Euler-Bernoulli beam theory for transverse impact problems [1, 5-6] may lead to some inaccuracy.

The equivalent plastic strain along the path of figure 8 is plotted in figure 9, for time $t^* = 101$ at $x/L = 0, 0.4, 0.67$ and 0.9 respectively. It can be observed that for impact locations $x/L = 0, 0.4, 0.67$ a full plastic hinge is developed, while for $x/L = 0.9$ only a partial plastic hinge is formed since the equivalent plastic strain in the range $-0.09 < 2z/h < 0$ is zero. The partial hinge is probably because of the lower impact energy at $x/L = 0.9$ and the fact that more of this energy is converted to kinetic energy in comparison to the other impact locations. The distribution is quite symmetric around the "neutral axis" since the stretching of the beam is very small.

The bending strain ε_{xx} along the length of the beams at $t^* = 101$ is plotted in figure 10, where the path is similar to that used for figure 5. The largest difference between the maximum bending strain of x / L = 0.0 and x/L = 0.9 is ~33%.

The equivalent plastic strain along the whole beam at $t^* = 101$ is plotted in figure 11. It can be observed that the impact at $x/L = 0$ results in a maximum equivalent plastic strain at the impact point of 2.8%, while for impact locations $-x/L = 0.4, 0.67, 0.9$ the maximum equivalent plastic strain is 1.9%, 1.8% and 1.3% respectively. For the impact location $x/L = 0$, four secondary partial hinges appear at symmetric locations $x/L = \pm 0.44$ and $x/L = \pm 0.74$. For impact location $x/L = -0.4$ three secondary partial hinges appear at locations $x/L = -0.79$ and $x/L = 0.39$ and $x/L = 0.78$. At , $x/L = -0.67$ there is only one secondary partial hinge at location $x/L = 0.65$. Finally, no secondary distinct hinges are observed for impact location $x/L = -0.9$ although considerable plastic deformation is evident at -0.8 < x / L < 0.7.

The secondary partial hinges develop long after the applied force has ceased to act. The equivalent plastic strain distribution along the beam impacted at x / L = 0 is plotted in

figure 12 for times $t^* = 5.05, 10.10, 15.15, 20.21$ and 101.0. The applied load (figure 3) becomes zero at about $t^* = 1.8$, while the first hinge at x/L = 0.73 starts to develop at $t^* = 5.05$ until full completion at $t^* = 10.10$. This hinge is in opposite direction to the main hinge at the impact location. The second hinge at x / L = 0.44 is not observed at $t^* = 10.10$ but is fully developed at $t^* = 15.15$. The deformed meshed beam with the equivalent plastic strain distribution at $t^* = 101$ near the partial hinge at x/L = 0.44 is shown in figure 13a. The equivalent plastic strain along the path seen in figure 13a is plotted in figure 13b. Figure 13 reveals that the inner half width of the beam remains elastic. For higher energy impacts this hinge would probably be fully plastic.

3.2.2 Energy partitioning

The applied impact energy (W_i) turns into kinetic (W_k) and internal energy (W_{in}). The internal energy consists of elastic strain energy (W_e) and plastically dissipated energy (W_p) : $W_{in} = W_e + W_p$. The energy is conserved and hence: $W_i = W_k + W_e + W_p$. The calculated applied impact energies were 33.3, 33.0, 34.0 and 25.3 J for impact locations x/L = 0, 0.4, 0.67 and 0.9 respectively. The kinetic energy of the striker is: $\frac{1}{2} m_s V_s^2 = 114.2$ J (m_s is the striker mass and $V_s = 33$ m/s is the striker velocity prior to the impact with the Hopkinson bar). It means that 22%-30% of the kinetic energy of the striker are applied to the beam. The beam maximum elastic strain energy capacity is calculated to be $W^e_{\max} = \frac{\sigma_y^2 V}{2E} = 46.4\ J$ (V being the beam's volume). The ratio

$R = \frac{W_i}{W^e_{\max}}$ [5] between the applied impact energy and the maximum elastic strain energy capacity of the beam is 0.72, 0.71, 0.73 and 0.55. The characteristic evolution of the different energies with time is shown in figure 14, in which the energy partitioning for impact location x/L = 0 is plotted. The energies are presented as percentage of the applied impact energy. In the early stage of loading, up to $t^* = 4$, most of the applied energy is converted to kinetic energy, but with time, the plastic deformation develops and the kinetic energy decreases. The kinetic energy is interchangeable with the elastic strain energy and their oscillations coincide for a large time. The plastic dissipation energy grows with time because the stress waves inside the beam continue to cause plastic deformations long after the applied force has become zero. The plastic dissipation energy remains constant for a time greater than $t^* = 65$, therefore, the plastic deformation process at $t^* = 101$ can be considered as completed as already mentioned. The sum of the internal and kinetic energies is equal to the applied energy as shown in figure 14 (for $t^* > 2$ when all energy has been applied since the results are normalized by the full applied energy and not the instantaneous applied energy).

The evolution of the elastic strain energy during the first $t^* = 101$ is plotted in figure 15. This energy fluctuates and is interchangeable with the kinetic energy. It can nevertheless be observed that for time range $65 < t^* < 101$, it varies between 2% - 16%. The average values over the time range $0 < t^* < 101$ are 10.7% , 9.9%, 10.1% and 13.9% for impact locations x/L = 0, 0.4, 0.67 and 0.9 respectively. This high relative elastic strain energy can not be neglected a-priori, and hence a full elastic plastic analysis is necessary and a

solution using plastic-rigid approach may be inaccurate. This supports the conclusions of [5].

The evolution of the kinetic energy for the four impact locations is plotted in figure 16. The average values over the time range $0 < t^* < 101$ are: 21.2%, 25.2% 35.2% and 43.2% for x/L = 0, 0.4, 0.67 and 0.9 respectively. It can be observed that when the impact location is less symmetrical, the kinetic energy increases since the impact increases the rotations.

The dissipated plastic work is plotted in figure 17. Dissipation reaches relative values of 76%, 71%, 59% and 52% of the total applied impact energy for impact locations x/L = 0, 0.4, 0.67 and 0.9 respectively. It is therefore clear that when the impact location is more symmetrical, the relative amount of the dissipated energy is higher, and hence more irreversible plastic damage will occur. The same conclusion has been reached in [6]. For symmetrical impact x / L = 0, the results of [6] are that 83% of the applied energy is dissipated plastically and 14% is converted to kinetic energy. The present study shows that 76% is dissipated and the kinetic energy for time greater than $t^* = 44.4$ *fluctuates* between 12% and 26% with an average of 21% for the first $t^* = 101$. This difference in the energy partitioning, although not huge, might be related of the use of different materials properties, different levels of applied energy (higher in [6]) and the simplified Kirchhoff assumptions used in [6] which were not used here.

4. Summary and Conclusions

Square, free-free aluminum alloy beams were impacted transversely at four different locations using a single Hopkinson bar setup. The strain gages readings during the impact

were recorded and used to determine the impact time-force curve. The dynamic response of the beams was investigated numerically. The numerical simulations were three-dimensional, transient, with an elastic plastic hardening material model. Moreover, large deformations were taken into account for arbitrarily shaped load functions that are obtained from the experiments. These aspects complement previous works [1-6].

An explicit finite elements solution [8] was applied to model four beams subjected to the transverse impacts at four different locations x/L = 0, 0.4, 0.67 and 0.9. The impact was simulated for a comparably long duration of t = 5 ms.

It was observed that when a square aluminum beam is transversely impacted, a stationary plastic hinge is created at the point of impact. This hinge is due to combined bending and stretching, where bending is the dominant mode. Most of the plastic deformation is confined to the impact zone $-1 < x/h < 1$. Impacts closer to the center of the beam (x/L = 0, 0.4) cause higher maximum plastic strains, when compared with impacts that are close to the free edge. Most of the plastic deformation occurs at the early stage of loading ($t^* < 4$) , but the propagating stress waves in the beam continue to deform it plastically up to a time of $t^* = 65$. Some distinct secondary partial plastic hinges are also observed to develop. The energy of the applied load was 0.55-0.73 of the maximum elastic energy capacity of the beam. This energy is comparably low and causes the elastic strain energy to an average 10%-14% of the total applied energy. Therefore, an elastic- plastic material model is necessary to model the impact, in accord with the conclusions of [5]. Moreover the nonlinear distribution of bending strains at the impact location (figure 8) indicates that the Euler-Bernouilli assumption might cause some inaccuracy in the results. The percentage of the applied energy which is converted to plastic deformation ranges from

72% for symmetric impact location to 52% for impact location of x / L = 0.9. The conclusion is that the more symmetric the impact location, the greater permanent plastic deformation. The kinetic energy is interchangeable with elastic strain energy and is not constant in time, but its averages ranges from 21% of the applied energy for symmetrical impact to 43% for impact location of x / L = 0.9.

The conclusions from this work are therefore that symmetrical impacts are more damaging to transversely impacted beams, even at relatively low impact energy levels. Unsymmetrical impacts, by contrast, will impart a higher kinetic energy to the beam. An elastic-plastic analysis is required to accurately model the beam's response. It also appears that the Euler-Bernouilli assumptions may induce some inaccuracy in the results.

References

[1] Jones, N., Structural Impact, Cambridge University press 1989, first paperback edition (with corrections) 1997.

[2] Lee, E. H., Symonds, P. S., Large plastic deformations of beam under transverse impact, J Appl Mech, 1952, pp. 308-314.

[3] Jones, N. and Wierzbicki, T., Dynamic plastic failure of a free-free beam , International Journal of Impact Engineering, 1987, vol. 6, no. 3, pp. 225-240.

[4] Yang J. L., Yu T. X., Reid S. R., Dynamic behaviour of a rigid perfectly plastic free-free beam subjected to step loading at any cross section along its span, Int J Impact Engng, 1998, vol. 21, No. 3, pp. 165-175.

[5] Yu, T. X., Yang, J. L., Reid, S. R. and Austin, C. D., Dynamic behavior of elastic-plastic free-free beams subjected to impulsive loading, Int. J. Solids Structures, 1996, vol. 33, No. 18, pp. 2659-2680.

[6] Yang J. L., Xi F., Experimental and theoretical study of free free beam subjected to impact at any cross section along its span, 2003, Int J Impact Engng, vol. 28, pp. 761-781.

[7] Kolsky, H., An investigation of the mechanical properties of materials at very high rates of loading, Proceeding of the Physical Society of London, 1949, 62B, pp. 676-700.

[8] ABAQUS/CAE version 6.6-1, Abaqus, Inc.

FIGURE CAPTIONS

Figure 1: The Aluminum beam with coordinate system.

Figure 2: The experimental setup. a. Sketch of the Hopkinson bar apparatus. b. A front view of the experimental .

Figure 3: Measured and numerically applied load for impact locations: $x/L = 0$, $x/L = 0.4$, $x/L = 0.67$ and $x/L = 0.9$.

Figure 4: a. A typical mesh at the edge of the beam. b. The square area on which a uniform pressure vs. time was applied to simulate the impact.

Figure 5: The transverse displacement u_z of the beams. a. impact location $x/L = 0$. b. impact location $x/L = -0.4$. c. impact location $x/L = -0.67$. d. impact location $x/L = -0.9$.

Figure 6: A cut view at impact location $x/L = 0$ of the deformed meshed beam showing the equivalent plastic strain distribution at $t^* = 101$. The strain distribution in the cross section shows a plastic hinge, whose extent along the beam is of about twice its width.

Figure 7: Evolution of equivalent plastic strain at point P of figure 6 for impact location $x/L = 0$. The plastic strain does not grow beyond $t^* = 65$.

Figure 8: Bending strain distribution , ε_x , along the thickness of the beam at impact location (the path in figure 6) for the four impact locations.

Figure 9: Equivalent plastic strain distribution along the thickness of the beam at impact location (the path in figure 6) for the four impact locations.

Figure 10: Bending strain distribution along the length of the beam at $(y/h, z/h) = (0, 1/2)$ at $t^* = 101$ for the four impact locations at which sharp peaks are noticeable.

Figure 11: Equivalent plastic strain distribution along the length of the beam at $(y/h, z/h) = (0, 1/2)$ at $t^* = 101$ for the four impact locations at which sharp peaks are noticeable.

Figure 12: Equivalent plastic strain distribution along the length of the beam at $(y/h, z/h) = (0, 1/2)$ at $t^* = 5.05, 10.10, 15.15, 20.21$ and 101.0 for impact location $x/L = 0$. The side peaks are characteristic of secondary plastic hinges.

Figure 13: A secondary partial plastic hinge at $x/L = 0.44$ for impact location $x/L = 0$ at $t^* = 101$. a. Equivalent plastic strain distribution along the beam. b. Equivalent plastic strain distribution along the path shown in figure 13a.

FIGURES

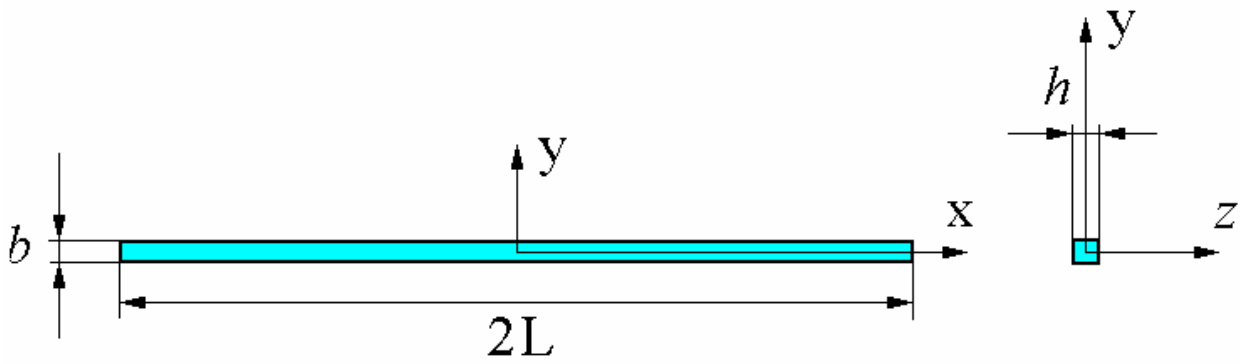

Figure 1: The aluminum beam with coordinate system.

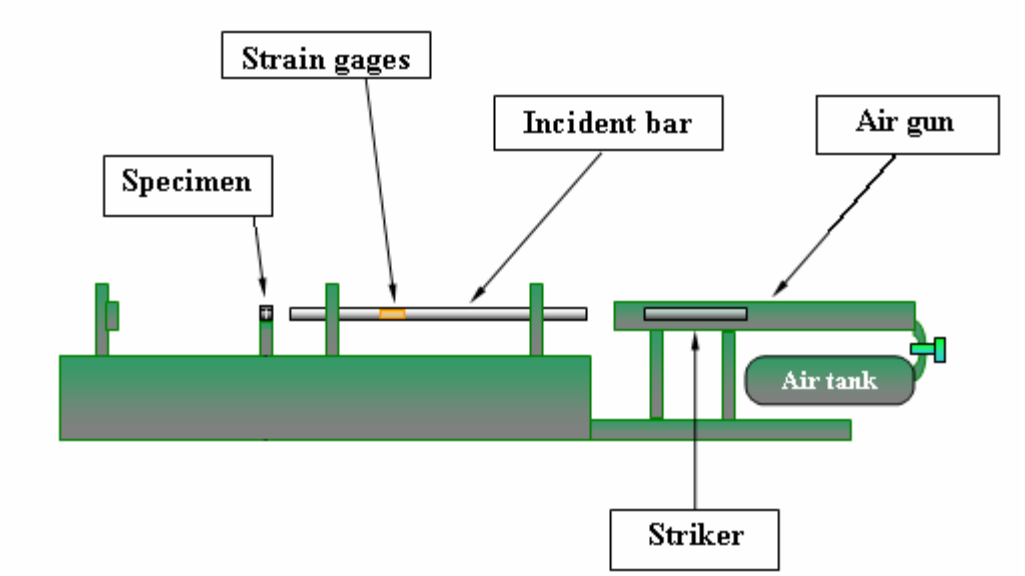

a.

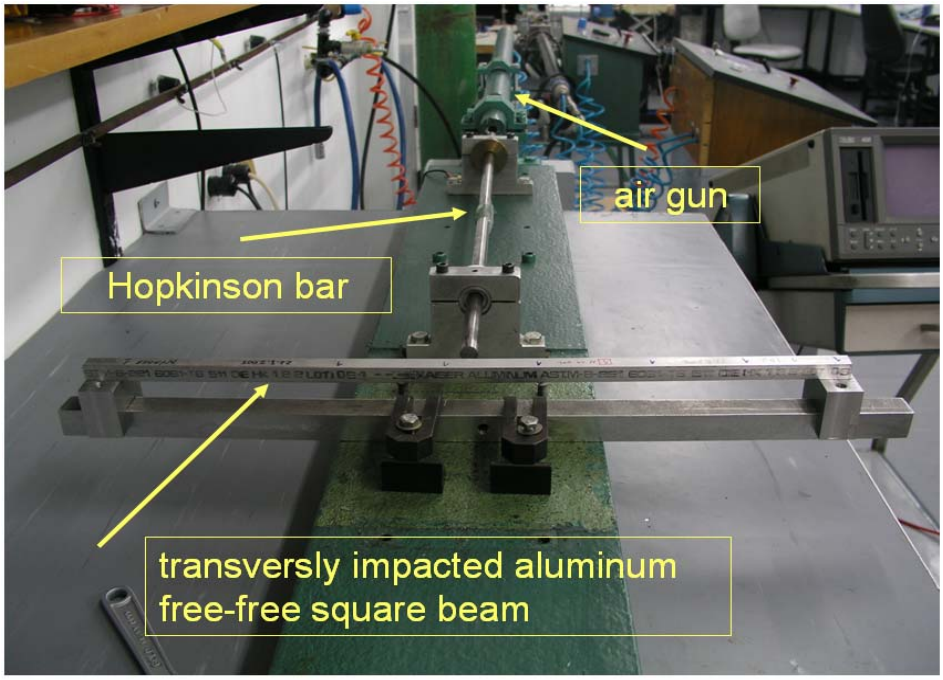

b.

Figure 2: The experimental setup. a. Sketch of the Hopkinson bar apparatus. b. A front view of the experimental setup.

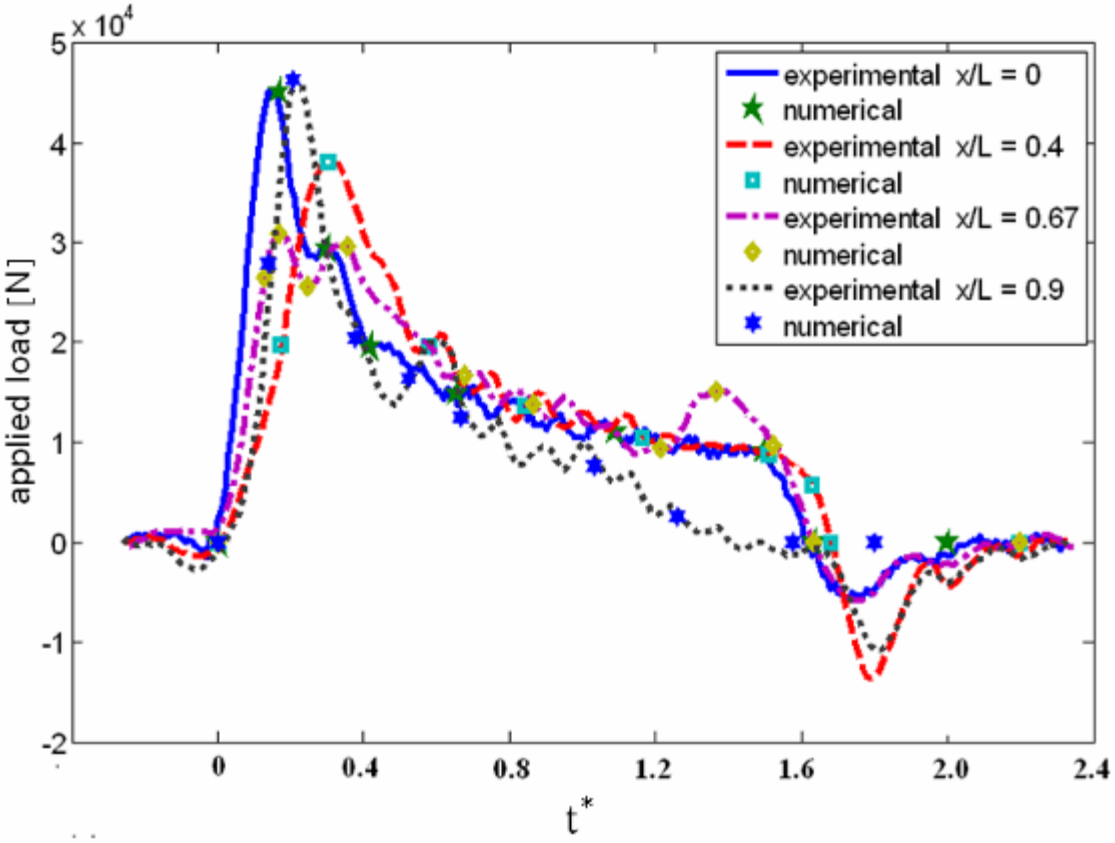

Figure 3: Measured and numerically applied load for impact locations: $x/L = 0$, $x/L = 0.4$, $x/L = 0.67$ and $x/L = 0.9$.

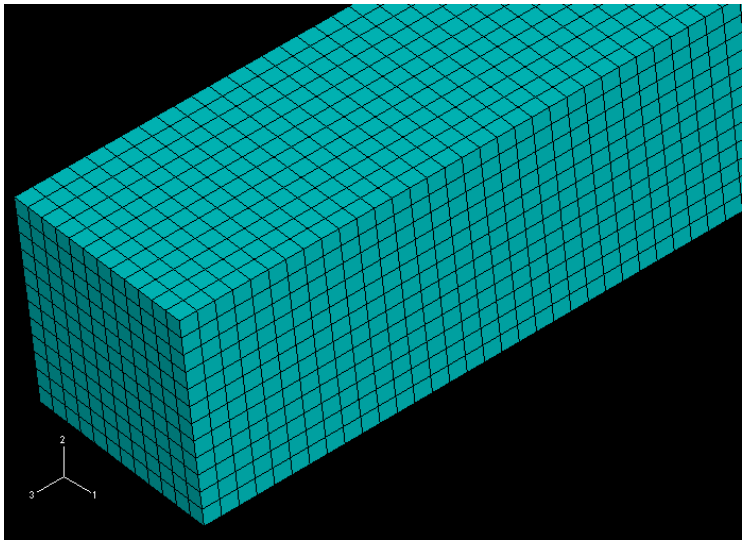

a.

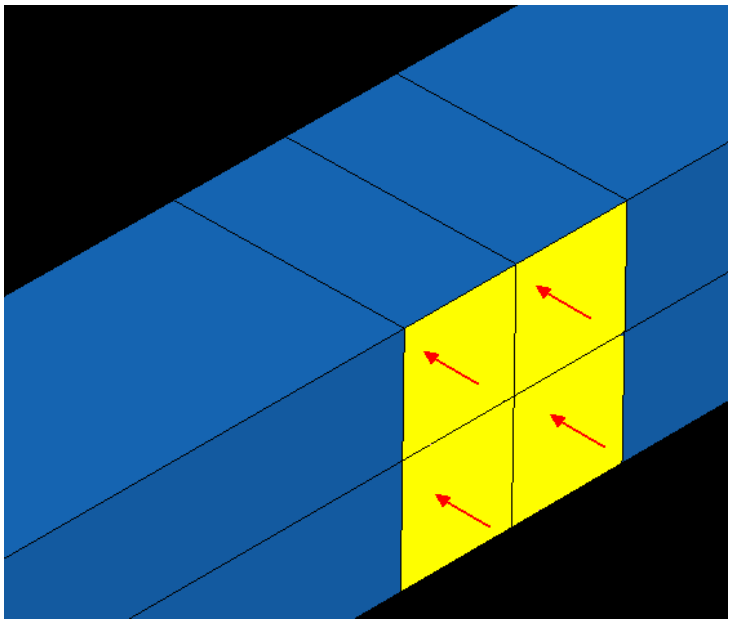

b.

Figure 4: a. A typical mesh at the edge of the beam. b. The square area on which a uniform pressure vs. time was applied to simulate the impact.

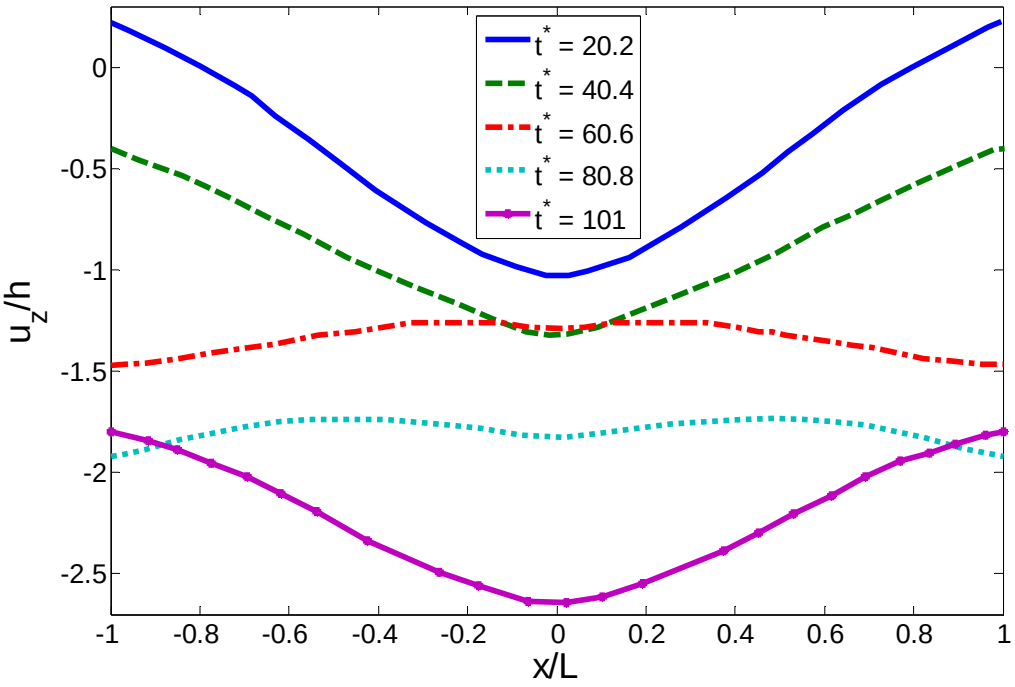
t* = 20.2
t* = 40.4
t* = 60.6
t* = 80.8
t* = 101
u_z/h
x/L
0
-0.5
-1
-1.5
-2
-2.5
-1
-0.8
-0.6
-0.4
-0.2
0
0.2
0.4
0.6
0.8
1

a.

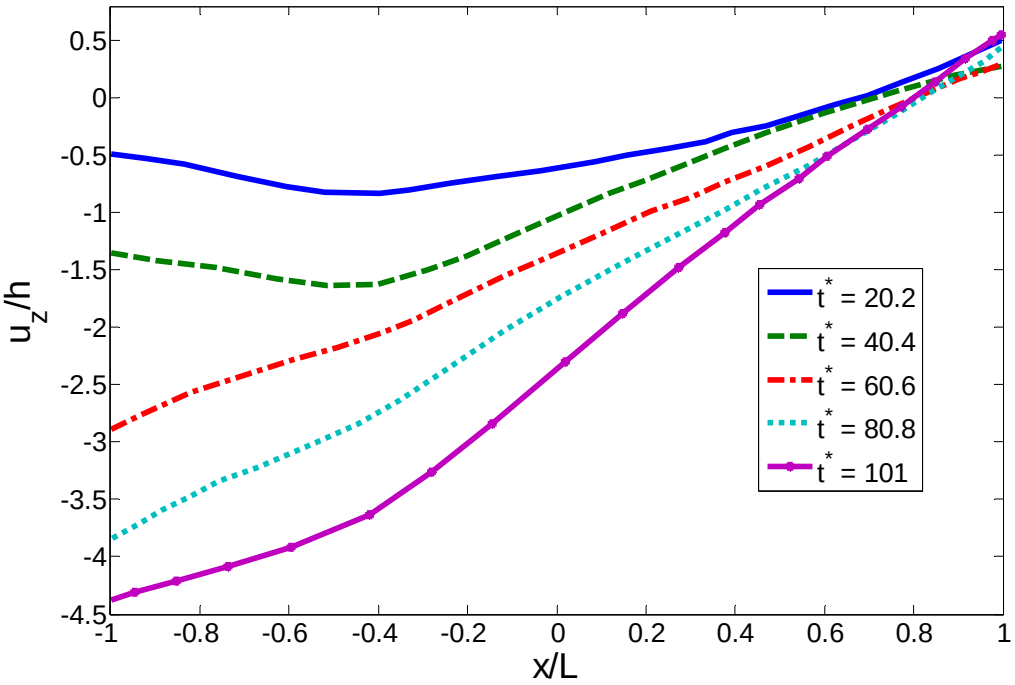
t* = 20.2
t* = 40.4
t* = 60.6
t* = 80.8
t* = 101
u_z/h
x/L
0.5
0
-0.5
-1
-1.5
-2
-2.5
-3
-3.5
-4
-4.5
-1
-0.8
-0.6
-0.4
-0.2
0
0.2
0.4
0.6
0.8
1

b.

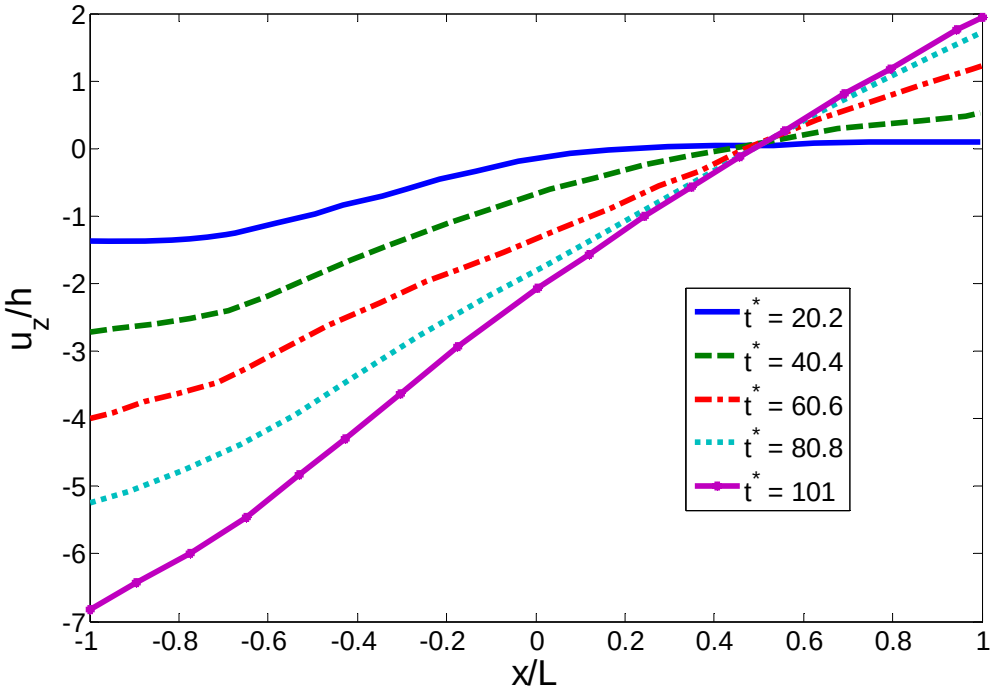

c.

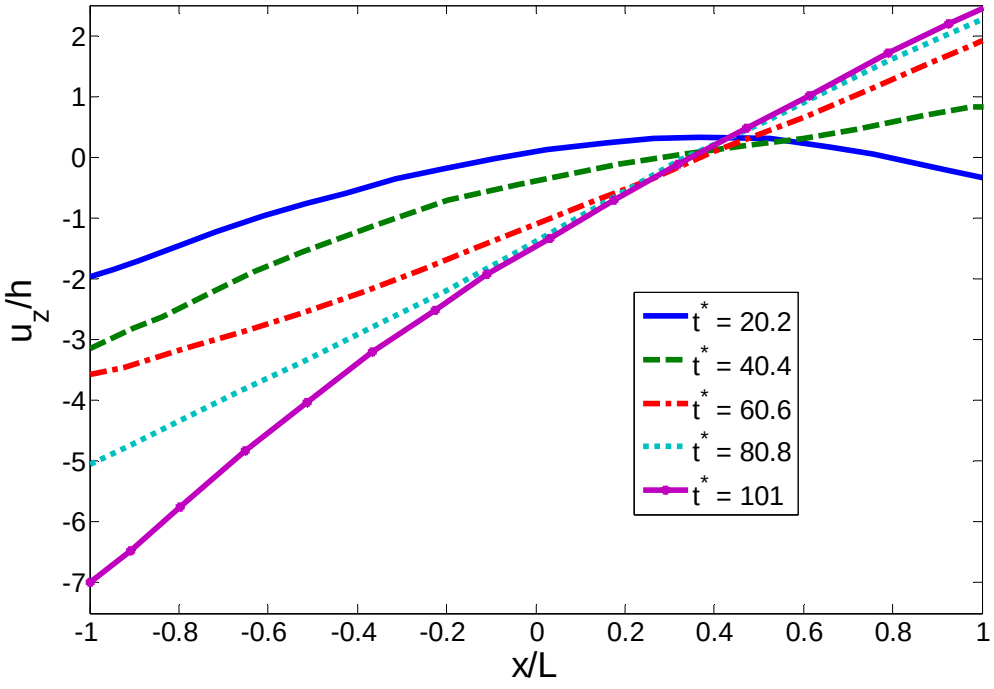

d.

Figure 5: The transverse displacement u_z of the beams. Impact locations are: a. $x/L = 0$. b. $x/L = -0.4$. c. $x/L = -0.67$. d. $x/L = -0.9$.

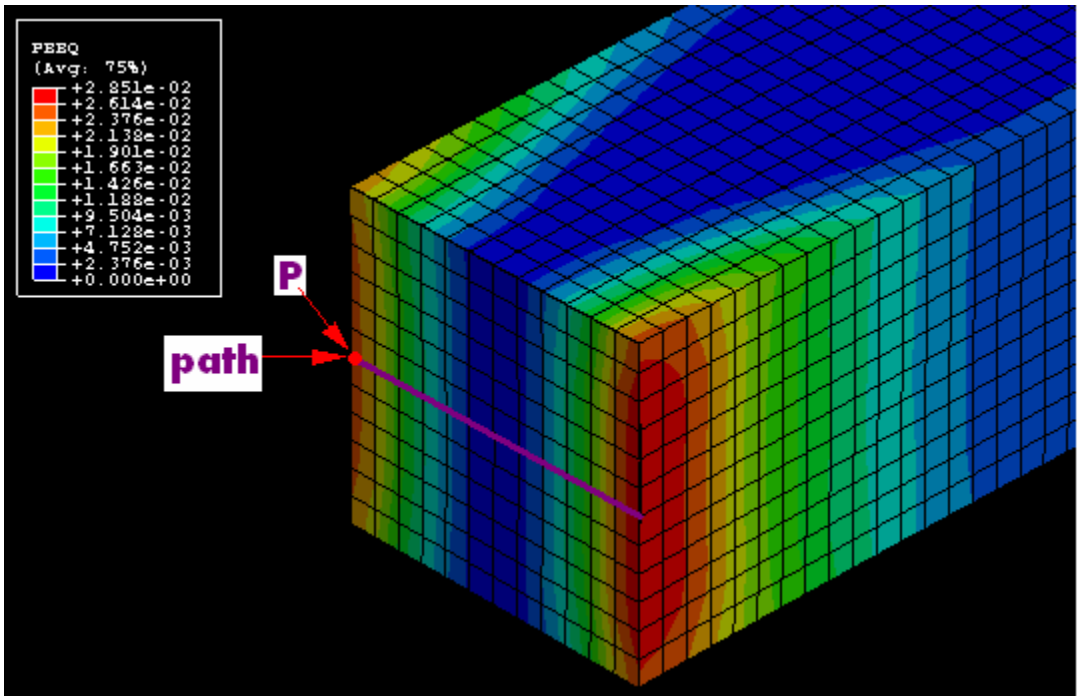

Figure 6: A cut view at impact location $x/L=0$ of the deformed meshed beam showing the equivalent plastic strain distribution at $t^{*}=101$. The strain distribution in the cross section shows a plastic hinge, whose extent along the beam is of about twice its width.

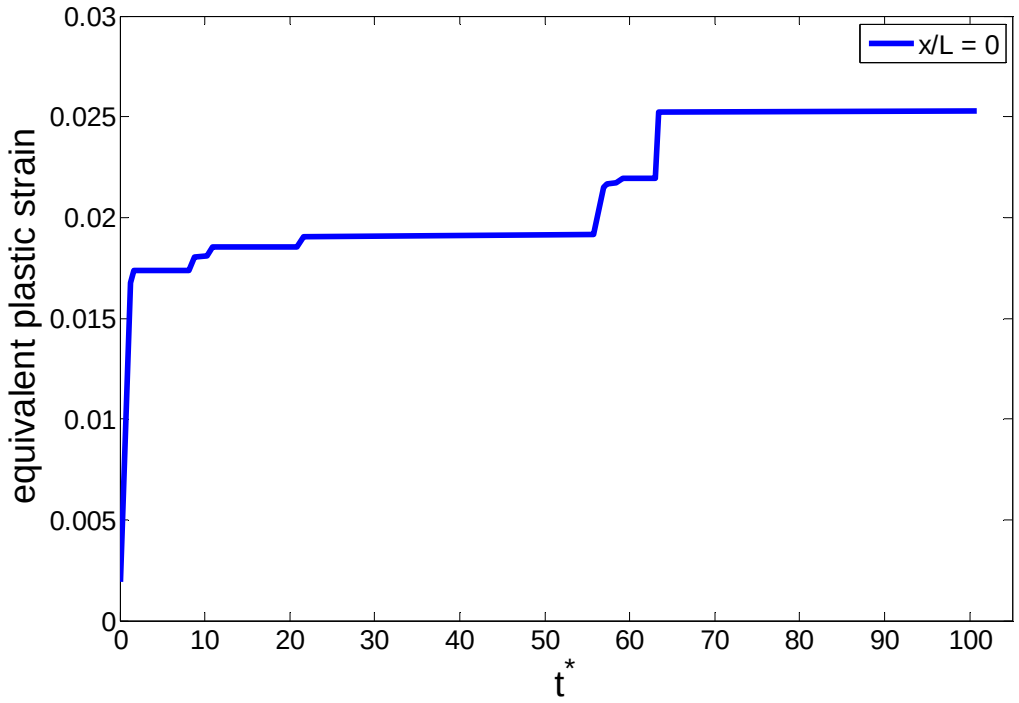

Figure 7: Evolution of equivalent plastic strain at point P of figure 6 for impact location x/L = 0. The plastic strain does not grow beyond $t^* = 65$.

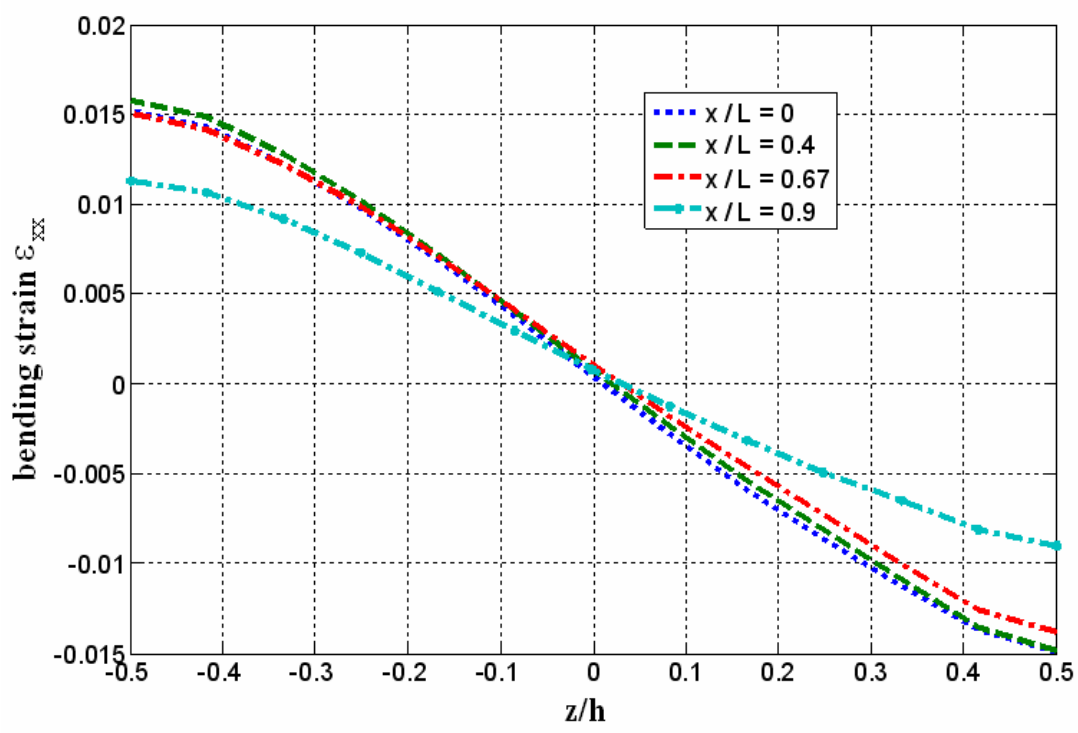

Figure 8: Bending strain distribution , ε_x , along the thickness of the beam at impact location (the path in figure 6) for the four impact locations.

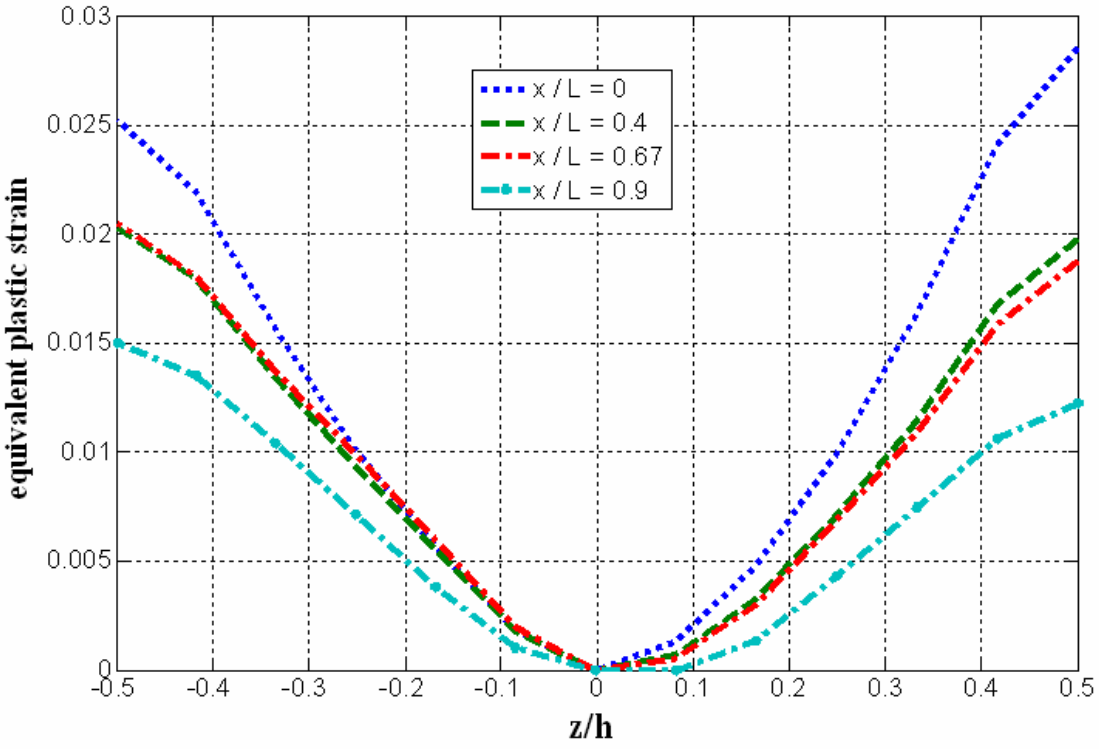

Figure 9: Equivalent plastic strain distribution along the thickness of the beam at impact location (the path in figure 6) for the four impact locations.

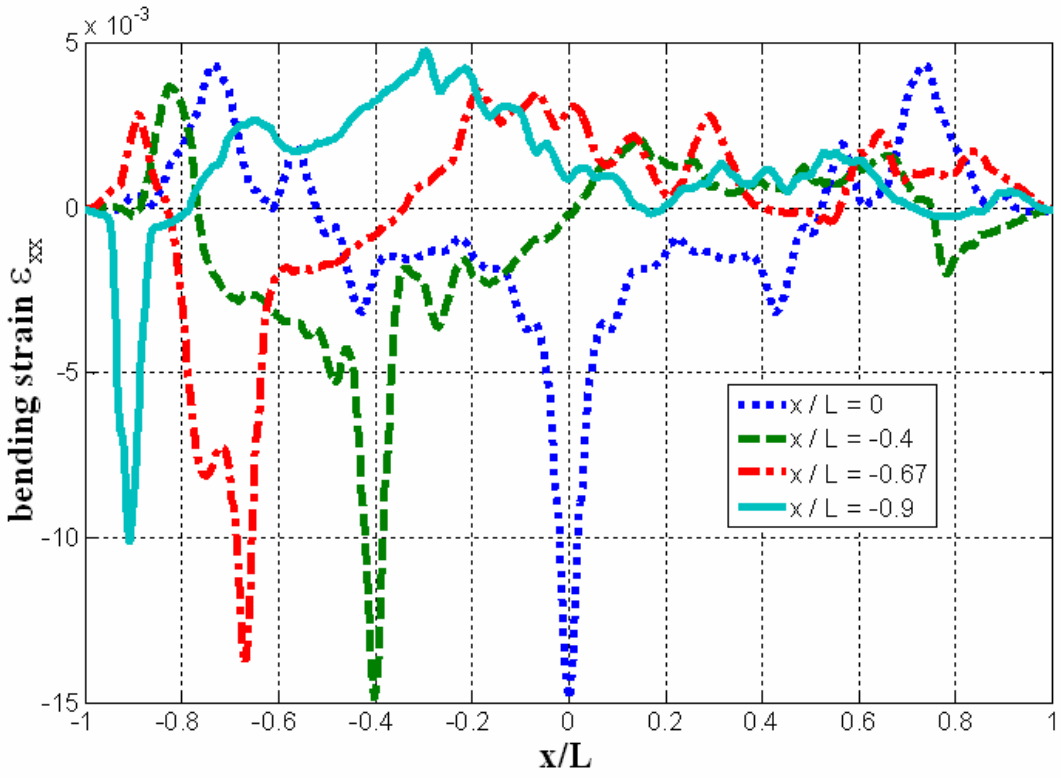

Figure 10: Bending strain distribution along the length of the beam at $(y/h, z/h) = (0, 1/2)$ at $t^* = 101$ for the four impact locations at which sharp peaks are noticeable.

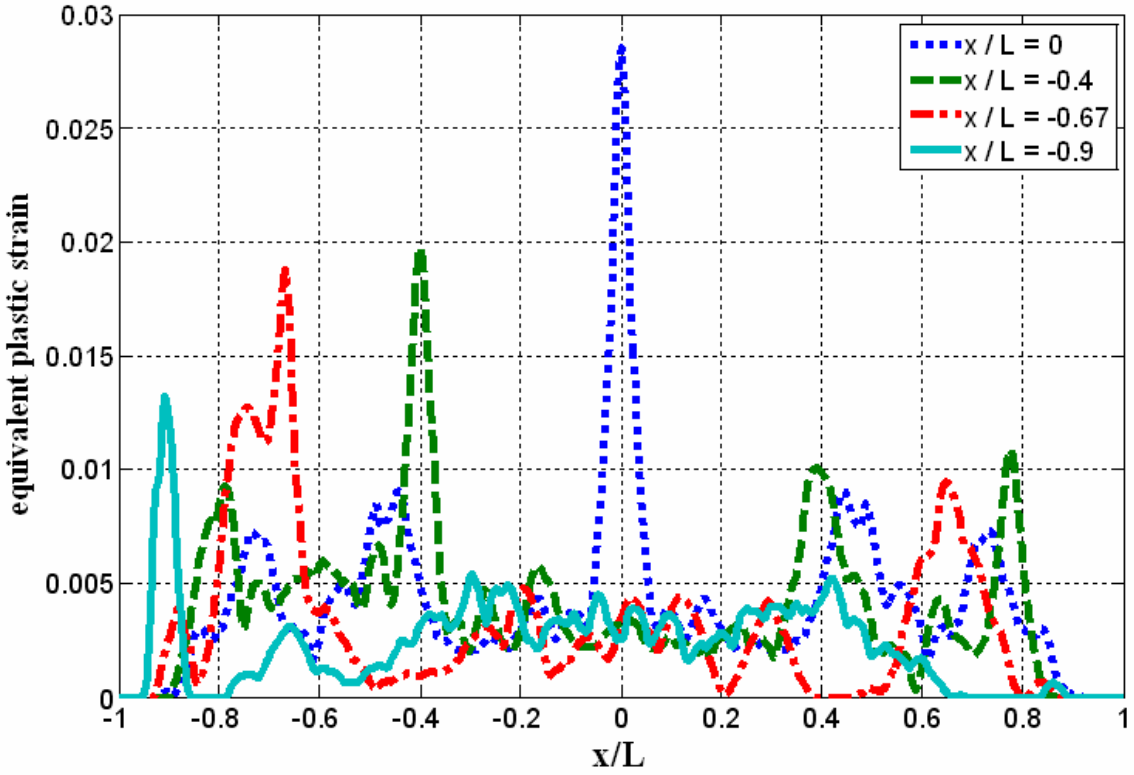

Figure 11: Equivalent plastic strain distribution along the length of the beam at $(y/h, z/h) = (0, 1/2)$ at $t^* = 101$ for the four impact locations at which sharp peaks are noticeable.

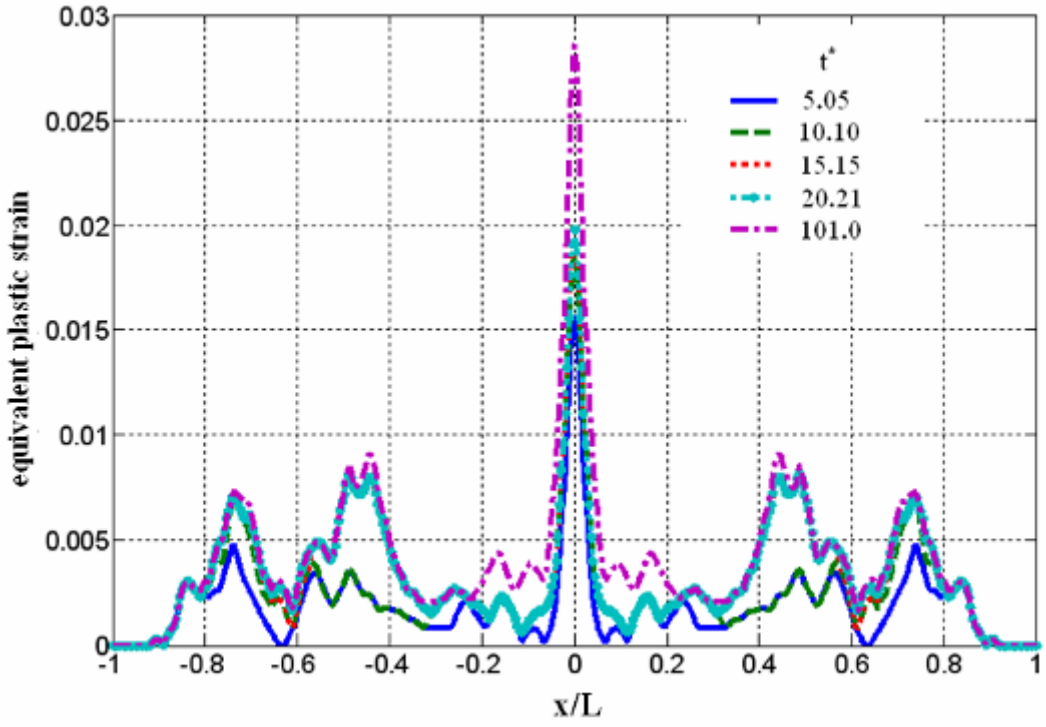

Figure 12: Equivalent plastic strain distribution along the length of the beam at $(y/h, z/h) = (0, 1/2)$ at $t^* = 5.05, 10.10, 15.15, 20.21$ and 101.0 for impact location $x/L = 0$. The side peaks are characteristic of secondary plastic hinges.

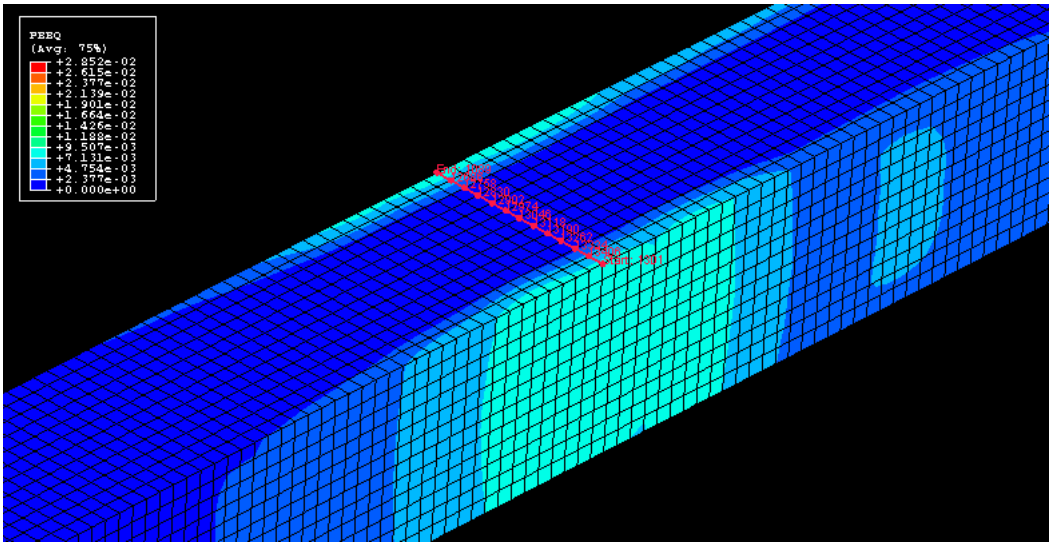

(a)

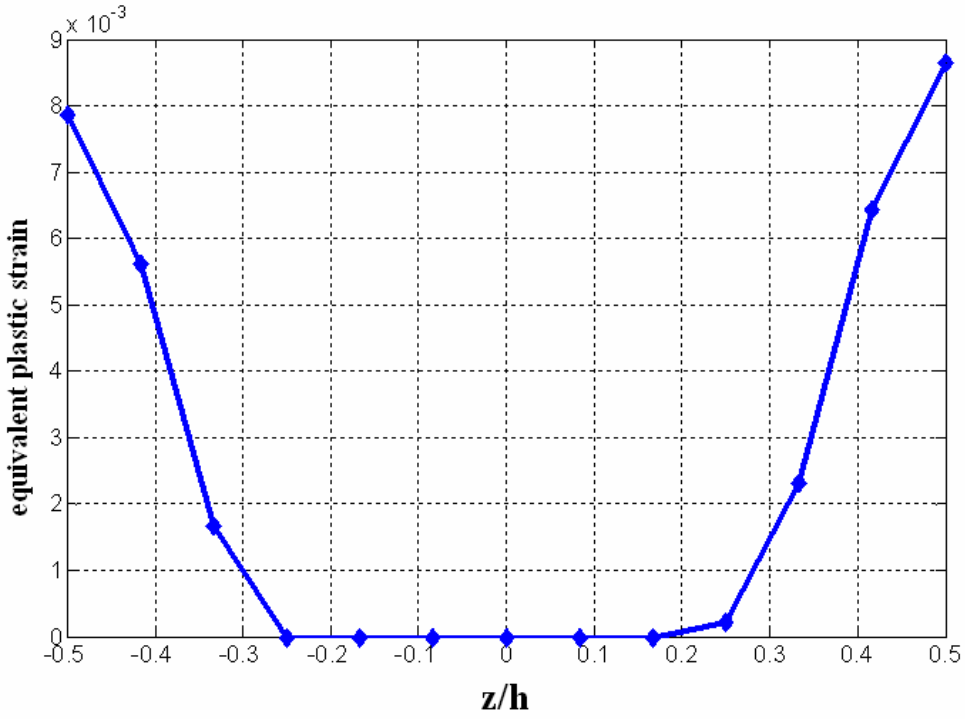

(b)

Figure 13: A secondary partial plastic hinge at $x / L = 0.44$ for impact location $x/L = 0$ at $t^* = 101$. a. Equivalent plastic strain distribution along the beam. b. Equivalent plastic strain distribution along the path shown in figure 13a.

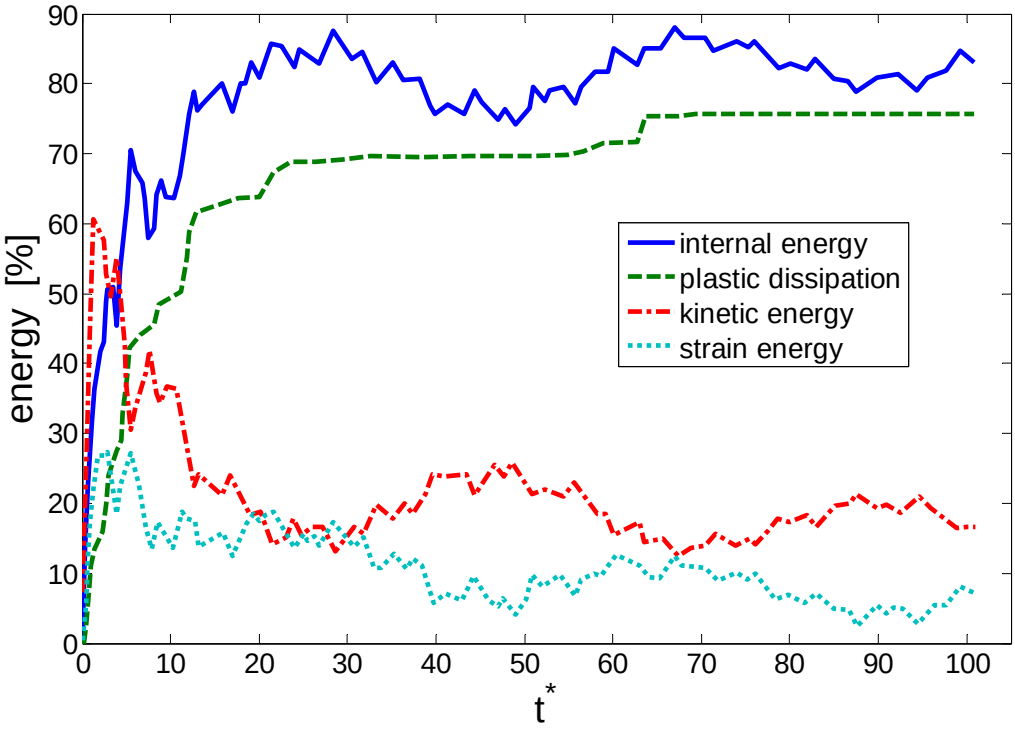

Figure 14: Normalized energy partitioning vs. time for impact location x / L = 0.

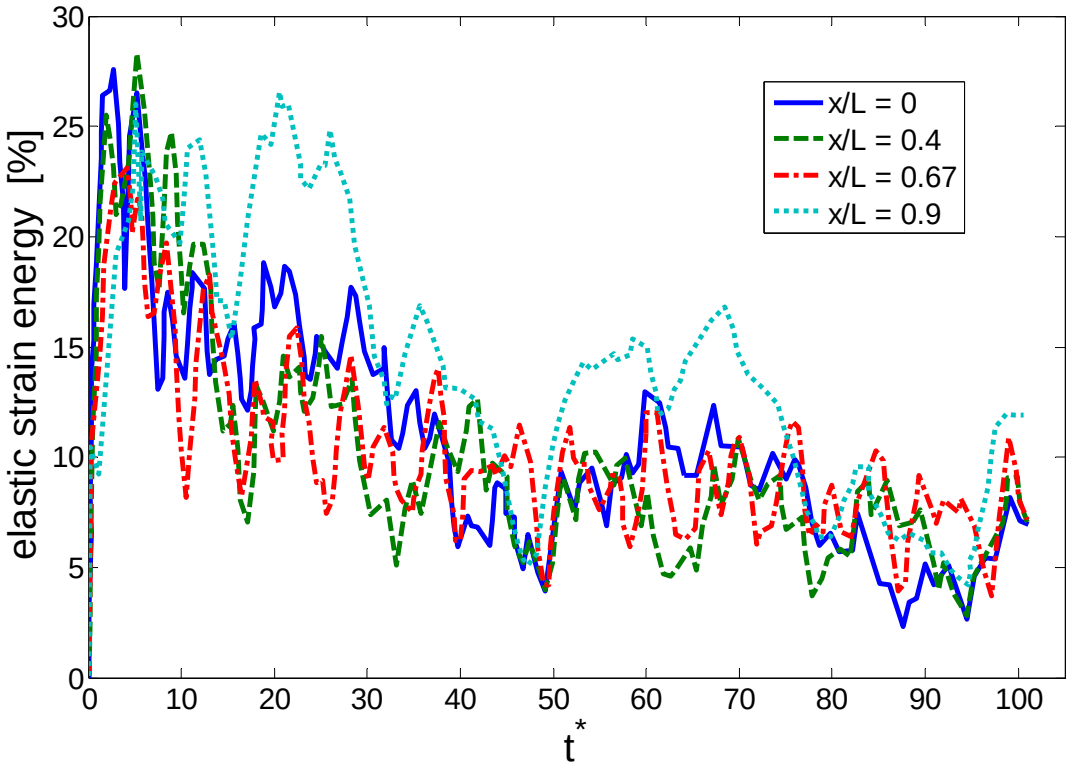

Figure 15: Elastic strain energy of the whole beam vs. time for the four impact locations.

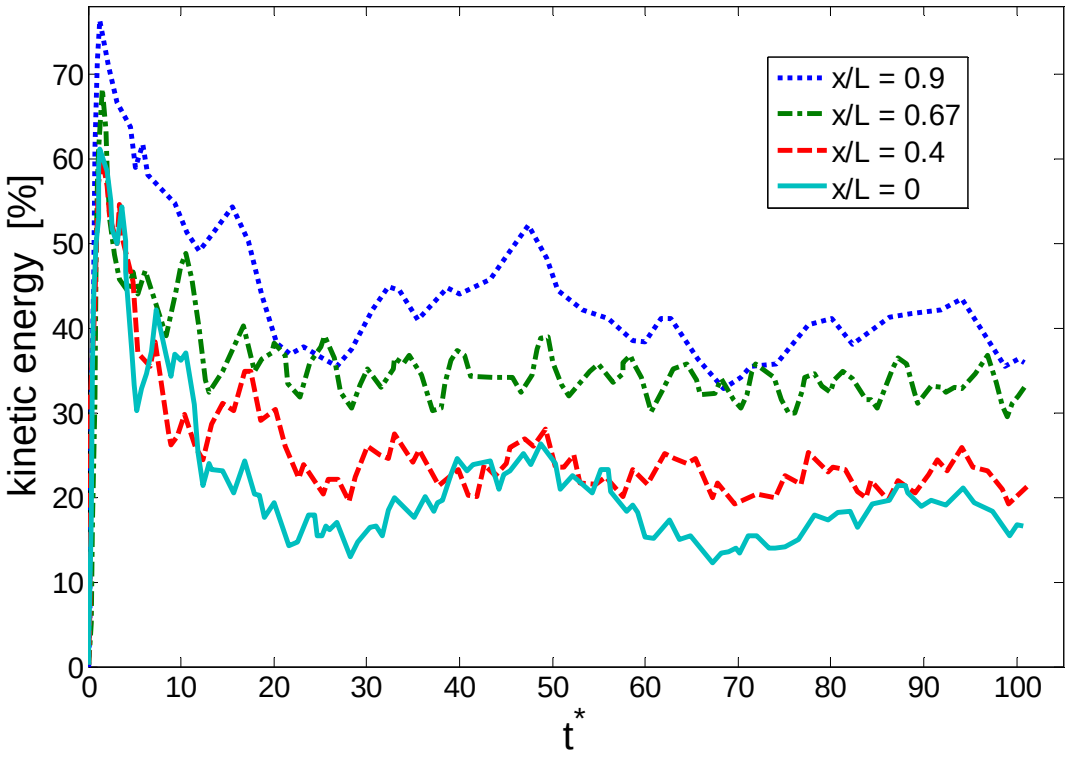

Figure 16: Kinetic energy of the whole beam vs. time for the four impact locations.

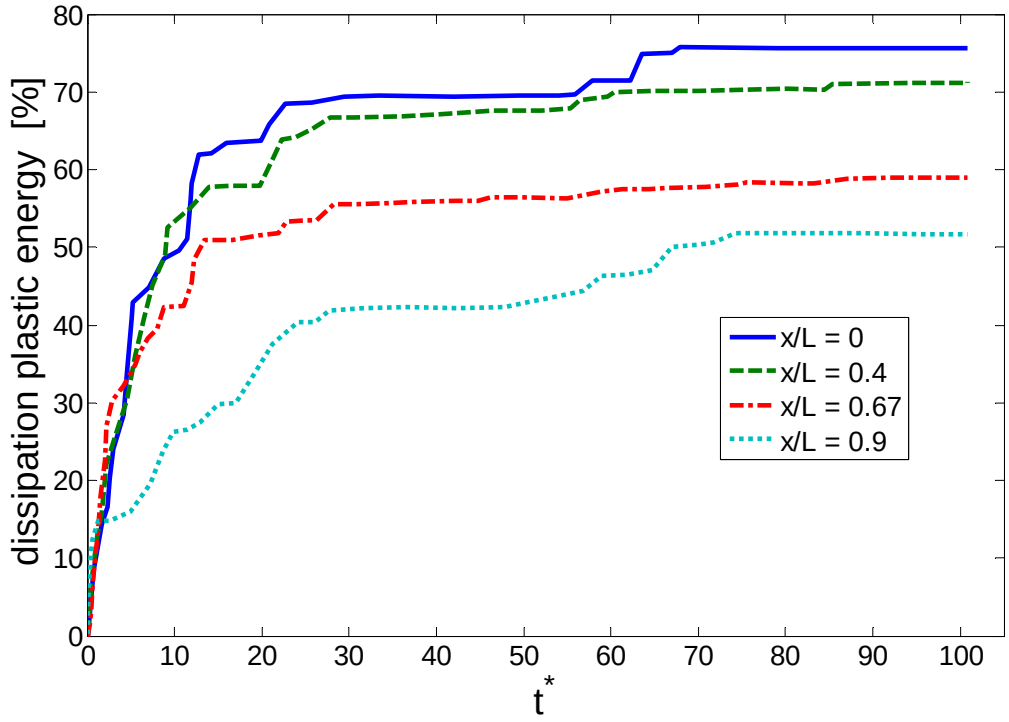

Figure 17: Plastic dissipation energy of the whole beam vs. time for the four impact locations.